Elastic nonlinear amplitude versus angle inversion and data-driven depth imaging in stratified media derived from inverse scattering approximations

2008 Inverse Problems 24 045006

(http://iopscience.iop.org/0266-5611/24/4/045006)

Inverse Problems **24** (2008) 045006 (23pp) doi:10.1088/0266-5611/24/4/045006

Elastic nonlinear amplitude versus angle inversion and data-driven depth imaging in stratified media derived from inverse scattering approximations

Lasse Amundsen[1,2], **Arne Reitan**[3], **Børge Arntsen**[1] **and Bjørn Ursin**[2]

[1] StatoilHydro Research Centre, Postuttak, N-7005 Trondheim, Norway
[2] Department of Petroleum Engineering and Applied Geophysics, The Norwegian University of Science and Technology, N-7491 Trondheim, Norway
[3] Professor emeritus, Skomakerveien 14, N-4839 Arendal, Norway

E-mail: lam@statoilhydro.com

Received 10 August 2007, in final form 5 May 2008
Published 10 June 2008
Online at stacks.iop.org/IP/24/045006

Abstract
This paper extends from acoustic to elastic the theory for nonlinear direct amplitude versus angle (AVA) inversion and data-driven depth imaging for a depth-variable medium published by the authors in this journal. The method which is derived by direct inversion of the forward model of elastic single compressional wave scattering requires no information of the velocities and density, except for the velocities and density of the uppermost layer which is the acoustic reference medium where the source and receiver are situated at finite distance above the elastic scattering medium. The vertically varying velocities and density of the scattering medium are estimated in a data-driven manner solely from the angle- and depth-dependent Born potential depth profile computed by constant-velocity imaging.

(Some figures in this article are in colour only in the electronic version)

1. Introduction

In reflection seismology a long-standing challenge has been to develop robust and reliable inverse methods that determine the subsurface medium parameters from reflection seismic data with a minimum or even no use of *a priori* information. General inverse geophysical methods have been the subject of many research papers since the 1970s. In particular, inverse scattering methods from the mainstream physics were introduced to the petroleum exploration industry during the late 1970s and early 1980s (see, e.g., Razavy (1975), Cohen and Bleistein (1979), Symes (1981) and Weglein *et al* (1981)). The recent developments presented by Weglein and coworkers (see, e.g., Weglein *et al* 2003) related to the inverse scattering series have stimulated new interest in formulating geophysical inversion in the language of scattering

0266-5611/08/045006+23$30.00

theory. The inverse problem, of course, is not unique to geophysics. One of the first scientists to treat the inverse problem was Lord Rayleigh, who considered in 1877 the problem of finding the density distribution of a string from knowledge of its vibrations. With the introduction of the Schrödinger equation to describe the quantum-mechanical model the problem of inverse scattering received high attention. Over the years, the inverse scattering procedures found widespread use in classical physics, where one of the most powerful non quantum-mechanical applications was in geophysics.

During recent years, inverse scattering theories related to seismic have been revisited and further developed. For an introduction to the inverse scattering series and results in the seismic field, the reader is referred to Weglein *et al* (2003, 2007), Innanen (2003) and Shaw (2005). Recently, Amundsen *et al* (2005, 2006) have addressed the 1D inverse scattering formalism, seeking approximate solutions to imaging objectives associated with primary scattering. For an acoustic layered medium Amundsen *et al* (2006) showed that the forward model derived in the WKBJ approximation can be inverted by following a three-step procedure. The current paper provides further insights into the inversion of the WKBJ forward model when the stratified medium is elastic with an acoustic top halfspace. To this end, the forward model derived in Amundsen *et al* (2006) must be extended from acoustic to elastic, and the inversion process must invert for both compressional and shear wave velocities in addition to density.

The paper is organized as follows. First, we derive the general physical forward model for P–P, P–S, S–P and S–S scattering for stratified media. Here, P and S refer to the compressional wave and shear wave, respectively. Then we derive the differential equation that governs single P–P scattering of elastic waves. The incident downgoing P-wave is described by the zero-order WKBJ approximation. The scattered P-wave is described by the first-order WKBJ approximation which takes into account the coupling of the incident wave with the scattered wave (Bremmer 1951, Ursin 1984). Second, the forward model is used as the mathematical framework for relating the angle-dependent Born potential to the single-scattering P–P response of a stratified elastic medium. Using the known constant velocity and density acoustic reference medium, the angle-dependent Born potential is simply obtained by trace integration of the scattered data transformed to the time intercept-slowness domain, by which the primary reflection events are placed at depths computed linearly only using the constant reference velocity and the travel times of primaries. Amplitude versus angle (AVA) analysis of the angle-dependent Born potential gives an estimate within the layer boundaries of the zero-angle Born potential depth profile what the depth-dependent velocity and density profiles are. Since the layer boundaries are severely mislocated in the zero-angle Born potential depth profile, the AVA analysis produces estimates of the amplitude of the actual velocity and density profiles but at wrong depths. We call the mislocated velocity and density profiles 'squeezed' profiles as they appear like the actual velocity and density profiles when the depth axis is squeezed. From the information in the squeezed P-wave velocity profile we show in the WKBJ approximation that the reflector positions in both the squeezed P-wave and S-wave velocity and squeezed density profiles can be moved with high precision towards their correct spatial location without introducing any information about the subsurface. Finally, a simple noise-free example is constructed to show how the procedures introduced in this paper can be applied to obtain the velocity and density profiles for the stratified elastic medium from its P–P scattering response.

2. The forward scattering model

In this section we present the forward model of elastic scattering. For a stratified medium it is standard procedure to transform the physical field variables by applying a Fourier transform with respect to horizontal spatial coordinates. This transforms the elastic equations into a system of first-order differential equations.

Let ω denote circular frequency and $\boldsymbol{x} = (x, y, z)$ the Cartesian coordinates. The depth axis is positive downwards. The horizontally layered elastic medium, where the P- and S-wave velocities $c_P = c_P(z)$ and $c_S = c_S(z)$, respectively, and density $\rho = \rho(z)$ are functions of depth, is embedded in a homogeneous reference medium with wave velocities c_{P0} and c_{S0} and density ρ_0. The wave-propagation velocities are related to the Lamé parameters, as $c_P = \sqrt{(\lambda + 2\mu)/\rho}$ and $c_S = \sqrt{\mu/\rho}$.

In the frequency-space domain, in a source-free region the system of equations governing the wave motion consists of the equation of motion,

$$-\mathrm{i}\omega\rho \tilde{V}_1 = \partial_1\tau_{11} + \partial_2\tau_{12} + \partial_3\tau_{13}, \tag{1}$$

$$-\mathrm{i}\omega\rho \tilde{V}_2 = \partial_1\tau_{21} + \partial_2\tau_{22} + \partial_3\tau_{23}, \tag{2}$$

$$-\mathrm{i}\omega\rho \tilde{V}_3 = \partial_1\tau_{31} + \partial_2\tau_{32} + \partial_3\tau_{33}, \tag{3}$$

and the constitutive relation,

$$-\mathrm{i}\omega\tau_{11} = \lambda(\partial_1\tilde{V}_1 + \partial_2\tilde{V}_2 + \partial_3\tilde{V}_3) + 2\mu\partial_1\tilde{V}_1, \tag{4}$$

$$-\mathrm{i}\omega\tau_{22} = \lambda(\partial_1\tilde{V}_1 + \partial_2\tilde{V}_2 + \partial_3\tilde{V}_3) + 2\mu\partial_2\tilde{V}_2, \tag{5}$$

$$-\mathrm{i}\omega\tau_{33} = \lambda(\partial_1\tilde{V}_1 + \partial_2\tilde{V}_2 + \partial_3\tilde{V}_3) + 2\mu\partial_3\tilde{V}_3, \tag{6}$$

$$-\mathrm{i}\omega\tau_{12} = -\mathrm{i}\omega\tau_{21} = \mu(\partial_2\tilde{V}_1 + \partial_1\tilde{V}_2), \tag{7}$$

$$-\mathrm{i}\omega\tau_{23} = -\mathrm{i}\omega\tau_{32} = \mu(\partial_3\tilde{V}_2 + \partial_2\tilde{V}_3), \tag{8}$$

$$-\mathrm{i}\omega\tau_{13} = -\mathrm{i}\omega\tau_{31} = \mu(\partial_1\tilde{V}_3 + \partial_3\tilde{V}_1), \tag{9}$$

where $\tau_{ij} = \tau_{ij}(\boldsymbol{x}, \omega)$ is the stress, $\tilde{V}_i = \tilde{V}_i(\boldsymbol{x}, \omega)$ is the particle velocity and ∂_i is the partial derivative operator with respect to x_i.

We take the particle-velocity vector $\tilde{\boldsymbol{V}}^T = (\tilde{V}_1, \tilde{V}_2, \tilde{V}_3)$ and the vertical-traction vector $\tilde{\boldsymbol{T}}^T = (\tilde{T}_1, \tilde{T}_2, \tilde{T}_3) = (\tau_{13}, \tau_{23}, \tau_{33})$ as the field quantities that characterize the elastic-wave propagation. Hence, the stresses $\tau_{11}, \tau_{22}, \tau_{12}$ must be algebraically eliminated from the above equations. To this end, substitute equation (6) for $\partial_3\tilde{V}_3$ into equations (4) and (5). Then, eliminate $\tau_{11}, \tau_{22}, \tau_{12}$ in equations (1) and (2) by using equations (4), (5) and (7). Bring ∂_3 terms to the left, all other terms to the right. By introducing the particle-velocity vertical-traction vector

$$\tilde{\boldsymbol{B}} = (\tilde{\boldsymbol{V}}^T, \tilde{\boldsymbol{T}}^T)^T, \tag{10}$$

the equation of motion and the constitutive relation can be written as an ordinary matrix-vector differential equation

$$\frac{\mathrm{d}}{\mathrm{d}z}\tilde{\boldsymbol{B}}(\boldsymbol{x}, \omega) = -\mathrm{i}\omega\tilde{\boldsymbol{A}}(z)\tilde{\boldsymbol{B}}(\boldsymbol{x}, \omega), \tag{11}$$

where the elastodynamic system matrix, $\tilde{\boldsymbol{A}}$, depending on material properties, has the form

$$\tilde{\boldsymbol{A}} = \begin{pmatrix} 0 & 0 & s\partial_x & \frac{1}{\mu} & 0 & 0 \\ 0 & 0 & s\partial_y & 0 & \frac{1}{\mu} & 0 \\ \frac{\lambda}{\lambda+2\mu}s\partial_x & \frac{\lambda}{\lambda+2\mu}s\partial_y & 0 & 0 & 0 & \frac{1}{\lambda+2\mu} \\ \rho - \theta s^2\partial_x^2 - \mu s^2\left(\partial_x^2 + \partial_y^2\right) & -\theta s^2\partial_x\partial_y & 0 & 0 & 0 & \frac{\lambda}{\lambda+2\mu}s\partial_x \\ -\theta s^2\partial_x\partial_y & \rho - \theta s^2\partial_y^2 - \mu s^2\left(\partial_x^2 + \partial_y^2\right) & 0 & 0 & 0 & \frac{\lambda}{\lambda+2\mu}s\partial_y \\ 0 & 0 & \rho & s\partial_x & s\partial_y & 0 \end{pmatrix}, \tag{12}$$

where $\theta = \mu(3\lambda + 2\mu)/(\lambda + 2\mu)$, and $s = (\mathrm{i}\omega)^{-1}$. The boundary conditions state continuity of $\tilde{\boldsymbol{B}}$ at welded interfaces. In addition, we impose the radiation conditions that the only downgoing wave in the source layer is that radiated by the source, and that there are no upgoing waves in the lower halfspace.

We introduce the Fourier transform with respect to horizontal spatial coordinates

$$G(k_x, k_y) = \int_{-\infty}^{\infty}\int_{-\infty}^{\infty} \mathrm{d}x\,\mathrm{d}y \exp[-\mathrm{i}(k_x x + k_y y)]\tilde{G}(x, y), \tag{13}$$

with inverse

$$\tilde{G}(x, y) = \frac{1}{(2\pi)^2}\int_{-\infty}^{\infty}\int_{-\infty}^{\infty} \mathrm{d}k_x\,\mathrm{d}k_y \exp[\mathrm{i}(k_x x + k_y y)]G(k_x, k_y). \tag{14}$$

Here, (k_x, k_y) are horizontal wavenumbers conjugate to (x, y). We introduce the radial wavenumber $k_r^2 = k_x^2 + k_y^2$, the horizontal slownesses $p_x = k_x/\omega$ and $p_y = k_y/\omega$, the radial slowness $p^2 = p_x^2 + p_y^2$, the P-wave vertical slowness $Q_P(z) = \sqrt{c_P^{-2}(z) - p^2}$ and the S-wave vertical slowness $Q_S(z) = \sqrt{c_S^{-2}(z) - p^2}$. In the reference medium the wavenumbers are denoted by $k_P = \omega/c_{P0}$ and $k_S = \omega/c_{S0}$, and the vertical slownesses are denoted by $q_P = \sqrt{c_{P0}{}^{-2} - p^2}$ and $q_S = \sqrt{c_{S0}{}^{-2} - p^2}$ for P- and S-waves, respectively. For notational convenience we define $\kappa_P = (c_{P0}q_P)^{-1}$ and $\kappa_S = (c_{S0}q_S)^{-1}$. In the reference medium, a plane P-wave is described by its frequency ω and direction of travel $\theta_P = \arcsin(c_{P0}p)$. The angle θ_P is measured as the ray's angle from the z-axis to the ray. Likewise, a plane S-wave of frequency ω has direction of travel $\theta_S = \arcsin(c_{S0}p)$. Then,

$$\kappa_P^{-1} = \cos\theta_P = \sqrt{1 - (c_{P0}p)^2},$$

and

$$\kappa_S^{-1} = \cos\theta_S = \sqrt{1 - (c_{S0}p)^2} = \sqrt{1 - \left(\frac{c_{S0}}{c_{P0}}\right)^2 \sin^2\theta_P}.$$

The Fourier transform of equation (11) leads to the first-order wave equation (Ursin 1983, Ikelle and Amundsen 2005)

$$\frac{\mathrm{d}}{\mathrm{d}z}\boldsymbol{B}(k_x, k_y, z) = -\mathrm{i}\omega\boldsymbol{A}(z)\boldsymbol{B}(k_x, k_y, z), \tag{15}$$

with field vector

$$\boldsymbol{B} = (\boldsymbol{V}^T, \boldsymbol{S}^T)^T, \tag{16}$$

and system matrix

$$\boldsymbol{A} = \begin{pmatrix} 0 & 0 & p_x & \frac{1}{\mu} & 0 & 0 \\ 0 & 0 & p_y & 0 & \frac{1}{\mu} & 0 \\ \frac{\lambda}{\lambda+2\mu}p_x & \frac{\lambda}{\lambda+2\mu}p_y & 0 & 0 & 0 & \frac{1}{\lambda+2\mu} \\ \rho - \theta p_x^2 - \mu p^2 & -\theta p_x p_y & 0 & 0 & 0 & \frac{\lambda}{\lambda+2\mu}p_x \\ -\theta p_x p_y & \rho - \theta p_y^2 - \mu p^2 & 0 & 0 & 0 & \frac{\lambda}{\lambda+2\mu}p_y \\ 0 & 0 & \rho & p_x & p_y & 0 \end{pmatrix}. \tag{17}$$

In the following we omit the field's dependence on wavenumbers.

To characterize the difference between the reference and actual media we introduce the P-wave velocity potential

$$\alpha_P(z) = 1 - \left(\frac{c_{P0}}{c_P(z)}\right)^2, \tag{18}$$

the S-wave velocity potential

$$\alpha_S(z) = 1 - \left(\frac{c_{S0}}{c_S(z)}\right)^2 \tag{19}$$

and the density potential

$$\alpha_\rho(z) = \ln r_\rho(z), \qquad r_\rho(z) = \frac{\rho_0}{\rho(z)}. \tag{20}$$

The P-wave vertical slowness now can be expressed as

$$Q_P(z) = q_P \Gamma_P(z),$$

where

$$\Gamma_P(z) = \left[1 - \kappa_P^2 \alpha_P(z)\right]^{\frac{1}{2}} \tag{21}$$

is a function of the P-wave potential and defines the ratio between the P-wave vertical slownesses in the actual and reference media. Likewise, the S-wave vertical slowness is expressed as

$$Q_S(z) = q_S \Gamma_S(z),$$

where

$$\Gamma_S(z) = \left[1 - \kappa_S^2 \alpha_S(z)\right]^{\frac{1}{2}} \tag{22}$$

is a function of the S-wave potential and defines the ratio between the S-wave vertical slownesses in the actual and reference media.

We now follow a notation close to Ikelle and Amundsen (2005). The field vector $\boldsymbol{B}$ can be decomposed into a wave vector

$$\boldsymbol{W} = [\boldsymbol{U}^T, \boldsymbol{D}^T]^T, \tag{23}$$

containing upgoing $\boldsymbol{U}^T = [U_P, U_{S_V}, U_{SH}]$ and downgoing $\boldsymbol{D}^T = [D_P, D_{S_V}, D_{SH}]$ waves by an eigensystem analysis of the system matrix $\boldsymbol{A}$. By inserting the flux-normalized eigenvectors of $\boldsymbol{A}$ into the columns of the 6×6 matrix $\boldsymbol{L}$, the up/down decomposition is achieved by the linear transformation

$$\boldsymbol{W} = \boldsymbol{L}^{-1}\boldsymbol{B}, \tag{24}$$

where

$$\boldsymbol{L}^{-1} = \boldsymbol{L}^{-1}(\boldsymbol{p}) = \begin{pmatrix} \boldsymbol{L}_{SU}^T(\boldsymbol{p}) & \boldsymbol{L}_{VU}^T(\boldsymbol{p}) \\ -\boldsymbol{L}_{SU}^T(-\boldsymbol{p}) & \boldsymbol{L}_{VU}^T(-\boldsymbol{p}) \end{pmatrix} \tag{25}$$

is the decomposition matrix, with $\boldsymbol{p} = (p_x, p_y)$, and

$$\boldsymbol{L} = \boldsymbol{L}(\boldsymbol{p}) = \begin{pmatrix} \boldsymbol{L}_{VU}(\boldsymbol{p}) & -\boldsymbol{L}_{VU}(-\boldsymbol{p}) \\ \boldsymbol{L}_{SU}(\boldsymbol{p}) & \boldsymbol{L}_{SU}(-\boldsymbol{p}) \end{pmatrix} \tag{26}$$

is the composition matrix. The 3×3 submatrices are

$$\boldsymbol{L}_{VU}(\boldsymbol{p}) = \frac{1}{\sqrt{2}} \begin{pmatrix} -p_x \frac{1}{\sqrt{\rho Q_P}} & \frac{p_x}{p}\sqrt{\frac{Q_S}{\rho}} & \frac{p_y}{p}\frac{1}{\sqrt{\mu Q_S}} \\ -p_y \frac{1}{\sqrt{\rho Q_P}} & \frac{p_y}{p}\sqrt{\frac{Q_S}{\rho}} & -\frac{p_x}{p}\frac{1}{\sqrt{\mu Q_S}} \\ \sqrt{\frac{Q_P}{\rho}} & p\frac{1}{\sqrt{\rho Q_S}} & 0 \end{pmatrix}, \tag{27}$$

$$
\boldsymbol{L}_{SU}(\boldsymbol{p}) = \frac{1}{\sqrt{2}} \begin{pmatrix} -2\mu p_x\sqrt{\frac{Q_P}{\rho}} & \frac{p_x}{p}(\rho - 2\mu p^2)\frac{1}{\sqrt{\rho Q_S}} & \frac{p_y}{p}\sqrt{\mu Q_S} \\ -2\mu p_y\sqrt{\frac{Q_P}{\rho}} & \frac{p_y}{p}(\rho - 2\mu p^2)\frac{1}{\sqrt{\rho Q_S}} & -\frac{p_x}{p}\sqrt{\mu Q_S} \\ (\rho - 2\mu p^2)\frac{1}{\sqrt{\rho Q_P}} & 2\mu p\sqrt{\frac{Q_S}{\rho}} & 0 \end{pmatrix}. \tag{28}
$$

The eigenvalue or vertical phase slowness $\gamma^{(N)}$ is determined by solving the determinantal equation

$$
\det\big(\boldsymbol{A} - \gamma^{(N)}\boldsymbol{I}\big) = 0. \tag{29}
$$

The six phase slownesses are given in pairs of opposite signs as

$$
\begin{aligned}
\gamma^{(1)} &= -\gamma^{(4)} = Q_P = \sqrt{c_P^{-2} - p^2}, \\
\gamma^{(2)} &= -\gamma^{(5)} = Q_S = \sqrt{c_S^{-2} - p^2}, \\
\gamma^{(3)} &= -\gamma^{(6)} = Q_S = \sqrt{c_S^{-2} - p^2}.
\end{aligned}
$$

2.1. *Differential equation for $\boldsymbol{W}$ in an inhomogeneous medium*

The differential equation for $\boldsymbol{W}$ in an inhomogeneous and source-free medium follows from equation (15) as

$$
\frac{\mathrm{d}\boldsymbol{W}(z)}{\mathrm{d}z} = [-\mathrm{i}\omega\boldsymbol{\Lambda}(z) + \boldsymbol{S}(z)]\,\boldsymbol{W}(z), \tag{30}
$$

where the eigenvalue decomposition of $\boldsymbol{A}$ gives the diagonal eigenvalue matrix

$$
\boldsymbol{\Lambda} = \boldsymbol{L}^{-1}\boldsymbol{A}\boldsymbol{L} = \mathrm{diag}[Q_P, Q_S, Q_S, -Q_P, -Q_S, -Q_S]. \tag{31}
$$

The scattering matrix which has a simple form due to flux-normalization of upgoing and downgoing waves is

$$
\boldsymbol{S}(z) = -\boldsymbol{L}^{-1}(z)\frac{\mathrm{d}\boldsymbol{L}(z)}{\mathrm{d}z} = \begin{pmatrix} \boldsymbol{S}_1(z) & \boldsymbol{S}_2(z) \\ \boldsymbol{S}_2(z) & \boldsymbol{S}_1(z) \end{pmatrix}, \tag{32}
$$

where

$$
\boldsymbol{S}_1(z) = \begin{pmatrix} 0 & s^+_{PSV}(z) & 0 \\ -s^+_{PSV}(z) & 0 & 0 \\ 0 & 0 & 0 \end{pmatrix}, \tag{33}
$$

and

$$
\boldsymbol{S}_2(z) = \begin{pmatrix} s_{PP}(z) & -s^-_{PSV}(z) & 0 \\ -s^-_{PSV}(z) & s_{SVSV}(z) & 0 \\ 0 & 0 & s_{SHSH}(z) \end{pmatrix}, \tag{34}
$$

with scattering coefficients

$$
s_{PP}(z) = \frac{1}{2}\left[\frac{\rho'(z)}{\rho(z)} - \frac{Q'_P(z)}{Q_P(z)} - 4p^2\frac{\mu'(z)}{\rho(z)}\right], \tag{35}
$$

$$
s_{SVSV}(z) = -\frac{1}{2}\left[\frac{\rho'(z)}{\rho(z)} - \frac{Q'_S(z)}{Q_S(z)} - 4p^2\frac{\mu'(z)}{\rho(z)}\right], \tag{36}
$$

$$s^{\pm}_{PSV}(z) = -\frac{1}{2}\frac{p}{\sqrt{Q_P(z)Q_S(z)}}\left[\frac{\rho'(z)}{\rho(z)} - 2(p^2 \pm Q_P(z)Q_S(z))\frac{\mu'(z)}{\rho(z)}\right], \tag{37}$$

$$s_{SHSH}(z) = -\frac{1}{2}\left[\frac{Q'_S(z)}{Q_S(z)} + \frac{\mu'(z)}{\mu(z)}\right], \tag{38}$$

where the prime denotes differentiation with respect to z. The scattering coefficients can be written as

$$s_{PP}(z) = -\frac{1}{2}\left[\frac{\mathrm{d}}{\mathrm{d}z}\ln[r_\rho(z)\Gamma_P(z)] + 4p^2\rho^{-1}(z)\frac{\mathrm{d}}{\mathrm{d}z}\mu(z)\right], \tag{39}$$

$$s_{SVSV}(z) = \frac{1}{2}\left[\frac{\mathrm{d}}{\mathrm{d}z}\ln[r_\rho(z)\Gamma_S(z)] + 4p^2\rho^{-1}(z)\frac{\mathrm{d}}{\mathrm{d}z}\mu(z)\right], \tag{40}$$

$$s^{\pm}_{PSV}(z) = \frac{1}{2}\frac{p}{\sqrt{q_Pq_S\Gamma_P(z)\Gamma_S(z)}}\left[\frac{\mathrm{d}}{\mathrm{d}z}r_\rho(z) + 2(p^2 \pm q_Pq_S\Gamma_P(z)\Gamma_S(z))\rho^{-1}(z)\frac{\mathrm{d}}{\mathrm{d}z}\mu(z)\right], \tag{41}$$

$$s_{SHSH}(z) = -\frac{1}{2}\frac{\mathrm{d}}{\mathrm{d}z}\ln\left[r_\mu^{-1}(z)\Gamma_S(z)\right]. \tag{42}$$

Equation (30) gives the differential equations for upgoing and downgoing P- and SV-waves, respectively,

$$\frac{\mathrm{d}}{\mathrm{d}z}U_P = -\mathrm{i}\omega Q_PU_P + s_{PP}D_P + s^{+}_{PSV}U_{SV} - s^{-}_{PSV}D_{SV}, \tag{43}$$

$$\frac{\mathrm{d}}{\mathrm{d}z}D_P = \mathrm{i}\omega Q_PD_P + s_{PP}U_P + s^{+}_{PSV}D_{SV} - s^{-}_{PSV}U_{SV}, \tag{44}$$

$$\frac{\mathrm{d}}{\mathrm{d}z}U_{SV} = -\mathrm{i}\omega Q_SU_{SV} + s_{SVSV}D_{SV} - s^{+}_{PSV}U_P - s^{-}_{PSV}D_P, \tag{45}$$

$$\frac{\mathrm{d}}{\mathrm{d}z}D_{SV} = \mathrm{i}\omega Q_SD_{SV} + s_{SVSV}U_{SV} - s^{+}_{PSV}D_P - s^{-}_{PSV}U_P. \tag{46}$$

The differential equations for upgoing and downgoing SH-waves are

$$\frac{\mathrm{d}}{\mathrm{d}z}U_{SH} = -\mathrm{i}\omega Q_SU_{SH} + s_{SHSH}D_{SH}, \tag{47}$$

$$\frac{\mathrm{d}}{\mathrm{d}z}D_{SH} = \mathrm{i}\omega Q_SD_{SH} + s_{SHSH}U_{SH}. \tag{48}$$

3. Single P–P wave scattering

Equations (43)–(46) are general differential equations for upgoing and downgoing coupled P- and SV-waves, and they describe all possible wave arrivals in the layered medium. Likewise, equations (47) and (48) are general differential equations for upgoing and downgoing SH-waves. In this paper, however, our interest is to describe single P–P scattering. To this end, we must describe the downward propagation of the incident P-wave field, and its interaction with the upward propagating single-scattered P-wave. Then, for the incident P-wave field we neglect the coupling of the upgoing with the downgoing mode as well as the coupling to SV-waves. Disregarding this interaction, which is called the zero-order WKBJ approximation, gives a one-way wave equation for the incident P-wave field. The single-scattered field is solved in the first-order WKBJ approximation, where the zero-order WKBJ approximation incident P-wave field is substituted into the differential equation for the upgoing P-wave field.

It is convenient to characterize the phase of the incident P-wave field in terms of the difference between wave propagation in models without and with the influence of the P-wave velocity potential. Therefore, we introduce the WKBJ shift function for the P-wave

$$\xi = \xi_P(z) = \int_{-\infty}^{z} \mathrm{d}z'[1 - \Gamma_P(z')] \tag{49}$$

which describes the phase difference between the unperturbed wave in the reference medium and the incident wave in the actual medium. The WKBJ shift function obeys the differential equation

$$-2\xi' + (\xi')^2 + \kappa_P^{-2}\alpha_P = 0, \qquad \xi^{(n)} = 0, \qquad n \geqslant 2. \tag{50}$$

The zero of the second- and higher-order derivatives of the shift function implies that it inside a layer must vary slowly over a wavelength.

3.1. *The incident P-wave field in the zero-order WKBJ approximation*

The one-way wave equation for the incident P-wave field is

$$\frac{\mathrm{d}D_P^{(0)}(z)}{\mathrm{d}z} = \mathrm{i}\omega q_P \Gamma_P(z) D_P^{(0)}(z), \tag{51}$$

with solution

$$D_P^{(0)}(z) = S_P(\omega)\exp(\mathrm{i}\omega q_P[z - \xi_P(z)]), \tag{52}$$

since the boundary condition states that just below the source, the downgoing field is that radiated by the source:

$$D_P^{(0)}(0^+) = S_P(\omega) = -\frac{a(\omega)}{2\mathrm{i}\omega q_P}, \tag{53}$$

where $a(\omega)$ is the source strength.

The reader should note that the differential equation (51) for the incident P-wave field does not depend on the scattering coefficient s_{PP}. This is purely an effect of flux-normalization of the upgoing and downgoing waves. If the upgoing and downgoing waves were amplitude normalized as in the acoustic one-way wave equation for the incident wave field presented in Amundsen *et al* (2006, equation (23)) the s_{PP}-coefficient would be present in the differential equation.

3.2. *P–P scattering in the first-order WKBJ approximation*

The differential equation for the single-scattered P-wave becomes

$$\frac{\mathrm{d}}{\mathrm{d}z} U_P^{(1)}(z) = -\mathrm{i}\omega q_P \Gamma_P(z) U_P^{(1)}(z) + s_{PP}(z) D_P^{(0)}(z). \tag{54}$$

Again, note that if the differential equation (54) is reduced to the acoustic model, it would differ slightly from the corresponding differential equation for the single-scattered acoustic wave presented in Amundsen *et al* (2006, equation (30)) due to the present flux-normalization.

Taking into account the radiation condition, $U_P(\infty) = 0$ (no scattered (upgoing) P-waves at infinity) the solution for the PP-scattered field at the measurement level is

$$U_P^{(1)}(z=0) = S_P(\omega)\int_0^\infty \mathrm{d}z\, s_{PP}(z)\exp(2\mathrm{i}\omega q_P[z-\xi_P(z)]). \tag{55}$$

It is convenient to express the scattered data in terms of the dimensionless scattering amplitude $\Phi_{PP} = S_P^{-1}U_P^{(1)}$. Our objective is to analyse the changes of the elastic parameters, and not their vertical derivatives. A partial integration of the log-derivative in equation (55) leads to the following result for the dimensionless scattering amplitude:

$$\Phi_{PP}(\omega) = -\frac{\mathrm{i}k_P}{2\kappa_P}\int_0^\infty \mathrm{d}z\,\alpha_{PP}(z)\exp(2\mathrm{i}\omega q_P[z-\xi_P(z)]), \tag{56}$$

where $\alpha_{PP}(z)$ is an angle-dependent P–P scattering potential

$$\alpha_{PP}(z) = -2\left[\ln[r_\rho(z)\Gamma_P(z)] - 2p^2[\mathrm{i}\omega q_P\Gamma_P(z)\rho(z)]^{-1}\frac{\mathrm{d}}{\mathrm{d}z}\mu(z)\right]\Gamma_P(z). \tag{57}$$

The P–P scattering potential contains the vertical derivative of the shear modulus. For the inversion of the data, however, we will discretize the shear modulus model in depth so that the shear modulus and shear wave velocity can be directly recovered.

Equation (56) is a nonlinear forward model for computing the dimensionless scattering amplitude $\Phi_{PP}(\omega)$ from the potential α_{PP}. We make the following remarks. The single-scattering amplitude is found by performing an integral over depth over the product of an amplitude function and a delay function. The amplitude function is the scattering potential. The delay function consists of the product of two functions, where the first $\exp(2\mathrm{i}\omega q_P z)$ accounts for two-way wave propagation of the unperturbed wave in the reference medium, whereas the second $\exp[-2\mathrm{i}\omega q_P\xi_P(z)]$ corrects for the influence of the potential. Since the scattered wave $U_P^{(1)}(z)$ travels through the same potential $\alpha_{PP}(z)$ as the incident wave $D_P^{(0)}(z)$ the shift function $\xi_P(z)$ is the same for both cases. For a piecewise-constant layered medium the delay function in the WKBJ approximation predicts the exact traveltimes of the single-scattering events. However, performing the integral over depth, the predicted amplitudes of the single-scattering events will not be exact for the piecewise-constant layered medium unless the boundary conditions of continuity of the vertical traction and the particle velocity at the interfaces are explicitly introduced. For the sake of forward modelling, the boundary conditions easily can be accounted for. Interfaces or discontinuities in the potential are then treated by correctly coupling the incident wave to the scattered waves. However, for the inverse problem, where the location of interfaces is not known, it would be cumbersome to account for the continuity conditions in an explicit manner. Therefore, as in Amundsen *et al* (2005, 2006) we neglect these conditions at the expense of using a forward model that predicts slightly incorrect amplitudes of the single-scattering events. The error can be analysed following the procedure as detailed in Amundsen *et al* (2005) for the 1D wave equation.

When we later simulate data to test the inverse scattering algorithm to be described in the following section, we do not base the simulation on the single-scattering forward model (56), but on an exact forward model for primary reflections in a piecewise-constant layered medium. This model is described in appendix A.

4. Inverse P–P scattering

In this section, we develop a procedure for reconstructing the velocity and density profiles from the dimensionless scattering amplitude Φ_{PP} recorded in an acoustic reference medium above an elastic stratified medium. As in the acoustic case described in Amundsen *et al* (2006) the elastic solution can be obtained in three steps. First, the angle-dependent Born potential α_{BPP} is computed from the scattered field in the time intercept-slowness domain using the constant reference medium. Second, we show that the squeezed P-wave velocity potential profile $\hat{\alpha}_P$, the related squeezed P-wave velocity profile $\hat{c}_P$, and the squeezed S-wave velocity and density profiles, $\hat{c}_S$ and $\hat{\rho}$, respectively, can be estimated from the residual moveout-corrected Born potential. Third, the squeezed profiles can be depth corrected by applying a nonlinear stretch function. The three steps require no information about the subsurface parameters except the reference medium parameters.

4.1. The angle-dependent Born potential and the single-scattering data

As in Amundsen *et al* (2006) we first establish a relationship between the angle-dependent Born potential and the single-scattering data. By the expression Born approximation it is understood that the exact incident P-wave is replaced by the incident P-wave $\exp(\mathrm{i}\omega q_P z)$ of the reference medium. In the forward model developed in this paper, the Born approximation translates to setting the shift function in the forward model (55) to zero,

$$\xi_P(z) \equiv 0. \tag{58}$$

In appendix C it is shown that Born forward model can be written as

$$\Phi_{PP}(\omega, p) = -\frac{\mathrm{i}\omega q_P}{2}\int_0^\infty \mathrm{d}z\,\alpha_{\mathrm{BPP}}(p, z)\exp(2\mathrm{i}\omega q_P z), \tag{59}$$

with single-scattering Born potential

$$\alpha_{\mathrm{BPP}}(z) = -2\ln[r_\rho(z)\Gamma_P(z) f_{\mu,\rho}(z)], \tag{60}$$

where

$$f_{\mu,\rho}(z) = \exp\left[4p^2\sum_{i=0}^{\infty}\frac{\Delta\mu(z_i)}{\rho(z_i)}H(z - z_i)\right], \tag{61}$$

and $H(z)$ is the Heaviside function.

To obtain the compact form of the Born potential, free of any vertical derivative of shear modulus, we have discretized the shear modulus model, with $z_i = i\Delta z$, such that

$$\mu(z) = \sum_{i=0}^{\infty}\Delta\mu(z_i)H(z - z_i), \tag{62}$$

where

$$\Delta\mu(z_i) = \mu(z_i) - \mu(z_{i-1}), \tag{63}$$

with derivative

$$\frac{\mathrm{d}}{\mathrm{d}z}\mu(z) = \sum_{i=0}^{\infty}\Delta\mu(z_i)\delta(z - z_i). \tag{64}$$

As shown in Amundsen *et al* (2006) the Born potential is obtained by constant-velocity migration or linear migration–inversion of the scattering data according to

$$\alpha_{\mathrm{BPP}}(p, z) = 4\int_{-\infty}^{2z/v_{P0}(p)}\mathrm{d}t\,\Phi_{PP}(t, p), \tag{65}$$

where $v_{P0} = c_{P0}/\sqrt{1 - (c_{P0}p)^2} = c_{P0}/\cos\theta_P$ is the apparent velocity in the reference medium of the plane wave along the depth axis.

Equation (65) is a key equation in the inversion procedure. In constant-velocity migration primary reflection events are placed at depths computed linearly using their traveltimes together with the constant reference velocity. In the following section, we shall see that the Born potential is the ticket for determining the values of elastic layered parameters.

4.2. Nonlinear AVA inversion: estimation of squeezed profiles $\hat{\alpha}_P$, $\hat{c}_P$, $\hat{c}_S$ and $\hat{\rho}$ from α_{BPP}

We now show that we can predict what the layer P-wave velocity, S-wave velocity, and density are, not as function of their true depth, but as function of the interface depths provided by the Born PP-wave potential at zero incidence angle. These profiles which are predicted from α_{BPP} at three different incidence angles are called 'squeezed' P-wave velocity, S-wave velocity and density profiles, denoted by $\hat{\alpha}_P$, $\hat{c}_P$, $\hat{c}_S$ and $\hat{\rho}$, respectively, because they can be seen as the profiles that would be obtained by compressing or squeezing the depth axis of the actual velocity and density profiles.

Before we proceed we make one remark. After constant-velocity imaging of the scattered data, one obtains one Born depth profile for every selected angle (or slowness). The first interface is always lined up at the correct depth, say z_1, in every Born depth profile. (The first primary travels in the reference medium only.) The second and following interfaces will show some residual moveout across the Born depth profiles. Since we aim at predicting the squeezed profiles $\hat{\alpha}_P$, $\hat{c}_P$, $\hat{c}_S$ and $\hat{\rho}$ as function of vertical depth from α_{BPP} at minimum three different incidence angles, the interface residual moveout must be corrected before the prediction can be done. The residual moveout correction does not affect the variation in amplitude with respect to angle of the Born potential.

Recalling that α_{BPP} is a function of radial slowness p, or equivalently, angle θ_P, we find

$$\alpha_{\mathrm{BPP}}(\theta_P, z) = -\ln\left(\hat{r}_\rho^2(z)[1-\sec^2\theta_P\hat{\alpha}_P(z)]\hat{f}_{\mu,\rho}^2(\theta_P, z)\right). \tag{66}$$

We make two comments. First, the relation between the Born potential and the squeezed velocity and density profiles is 'exact' within the limitations of the forward model which among others assumes perfect transmission. Further, the relation is nonlinear; it is not linearized in any way with respect to changes in the elastic parameters as is commonly done in seismic amplitude versus angle analysis. Second, the relationship has not been derived by assuming that the single scattering is from a smoothly changing medium. Interfaces with step-discontinuities in the medium parameters can be (and is) present. Thus, there is no requirement of small contrasts in the elastic parameters across interfaces. Therefore, the relation (66) is the ticket to determining the elastic parameters.

From equation (66) it follows that

$$\hat{r}_\rho^2(z)\hat{f}_{\mu,\rho}^2(\theta_P, z)[1-\sec^2\theta_P\hat{\alpha}_P(z)] = \exp[-\alpha_{\mathrm{BPP}}(\theta_P, z)]. \tag{67}$$

When the Born depth profile is known for three angles of incidence θ_{P0}, θ_{P1} and θ_{P2}, the squeezed P-wave velocity potential is the solution of the algebraic equation

$$\begin{aligned}\left(\frac{1-\sec^2\theta_{P2}\hat{\alpha}_P(z)}{1-\sec^2\theta_{P1}\hat{\alpha}_P(z)}\right)^{\sin^2\theta_{P0}}&\left(\frac{1-\sec^2\theta_{P0}\hat{\alpha}_P(z)}{1-\sec^2\theta_{P2}\hat{\alpha}_P(z)}\right)^{\sin^2\theta_{P1}}\left(\frac{1-\sec^2\theta_{P1}\hat{\alpha}_P(z)}{1-\sec^2\theta_{P0}\hat{\alpha}_P(z)}\right)^{\sin^2\theta_{P2}}\\ &= \exp[(\sin^2\theta_{P0}-\sin^2\theta_{P2})(\alpha_{\mathrm{BPP}}(\theta_{P1}, z)-\alpha_{\mathrm{BPP}}(\theta_{P0}, z))\\ &\quad -(\sin^2\theta_{P0}-\sin^2\theta_{P1})(\alpha_{\mathrm{BPP}}(\theta_{P2}, z)-\alpha_{\mathrm{BPP}}(\theta_{P0}, z))]\end{aligned} \tag{68}$$

which can iteratively be solved by Newton's method. The associated squeezed P-wave velocity profile is

$$\hat{c}_P(z) = c_{P0}[1-\hat{\alpha}_P(z)]^{-\frac{1}{2}}. \tag{69}$$

From the Born depth profile at $\theta_{P0} = 0$ and the estimated squeezed velocity potential profile $\hat{\alpha}_P$, the density ratio straightforwardly can be computed as

$$\frac{\hat{\rho}(z)}{\rho_0} = \hat{r}_\rho^{-1}(z) = [1-\hat{\alpha}_P(z)]^{\frac{1}{2}}\exp\left[\frac{1}{2}\alpha_{\mathrm{BPP}}(\theta_{P0}=0, z)\right]. \tag{70}$$

The shear modulus can be estimated from the equation

$$\hat{f}_{\mu,\rho}(z) = \left(\frac{\exp[-\frac{1}{2}\alpha_{\mathrm{BPP}}(\theta_{P1}, z)]}{\hat{r}_\rho(z)[1 - \sec^2\theta_{P1}\hat{\alpha}_P(z)]^{\frac{1}{2}}}\right), \tag{71}$$

where $\theta_{P1} \neq 0$. This gives

$$\sum_i \frac{\Delta\mu(z_i)}{\rho(z_i)} H(z - z_i) = \left(\frac{c_{P0}}{2\sin\theta_{P1}}\right)^2 \ln\left(\frac{\exp\left[-\frac{1}{2}\alpha_{\mathrm{BPP}}(\theta_{P1}, z)\right]}{\hat{r}_\rho(z)[1 - \sec^2\theta_{P1}\hat{\alpha}_P(z)]^{\frac{1}{2}}}\right). \tag{72}$$

By letting $z^- = z - \Delta z$ the S-wave velocity estimate is given from the equation

$$\begin{aligned} c_S^2(z) = \frac{\rho(z^-)}{\rho(z)} c_S^2(z^-) + \left(\frac{c_{P0}}{2\sin\theta_{P1}}\right)^2 \ln\left[\frac{\rho(z)}{\rho(z^-)}\left(\frac{1 - \sec^2\theta_{P1}\hat{\alpha}_P(z^-)}{1 - \sec^2\theta_{P1}\hat{\alpha}_P(z)}\right)^{\frac{1}{2}}\right. \\ \left.\times \exp\left(\frac{1}{2}[\alpha_{\mathrm{BPP}}(\theta_{P1}, z^-) - \alpha_{\mathrm{BPP}}(\theta_{P1}, z)]\right)\right]. \end{aligned} \tag{73}$$

4.3. Residual depth imaging: stretching of the squeezed profiles towards the actual profiles

The nonlinear AVA analysis has determined the squeezed velocity potential $\hat{\alpha}_P$ and the squeezed P-wave velocity, S-wave velocity and density, $\hat{c}_P, \hat{c}_S$ and $\hat{\rho}$, respectively. The residual depth imaging step for the elastic data is identical to that for acoustic data developed in Amundsen *et al* (2006). Residual depth imaging of the velocity and density profiles is given as, respectively,

$$\hat{\alpha}_P(z) = \alpha_P\left(z + \int_{-\infty}^{z} \mathrm{d}z'[(1 - \hat{\alpha}_P(z'))^{-\frac{1}{2}} - 1]\right), \tag{74}$$

$$\hat{c}_P(z) = c_P\left(z + \int_{-\infty}^{z} \mathrm{d}z'[(1 - \hat{\alpha}_P(z'))^{-\frac{1}{2}} - 1]\right) = c_P\left(c_{P0}^{-1}\int_{-\infty}^{z} \mathrm{d}z'\hat{c}_P(z')\right), \tag{75}$$

$$\hat{c}_S(z) = c_S\left(z + \int_{-\infty}^{z} \mathrm{d}z'[(1 - \hat{\alpha}_P(z'))^{-\frac{1}{2}} - 1]\right) = c_S\left(c_{P0}^{-1}\int_{-\infty}^{z} \mathrm{d}z'\hat{c}_P(z')\right) \tag{76}$$

and

$$\hat{\rho}(z) = \rho\left(z + \int_{-\infty}^{z} \mathrm{d}z'[(1 - \hat{\alpha}_P(z'))^{-\frac{1}{2}} - 1]\right) = \rho\left(c_{P0}^{-1}\int_{-\infty}^{z} \mathrm{d}z'\hat{c}_P(z')\right). \tag{77}$$

Thus, provided that the Born potential has been computed according to equation (65), then equations (74)–(77) suggest a two-step procedure for estimating the medium. First, the squeezed profiles $\hat{\alpha}_P, \hat{c}_P, \hat{c}_S$ and $\hat{\rho}$ are estimated by nonlinear AVA analysis of the Born potential. Then the actual velocity and density profiles α_P, c_P, c_S, and ρ are derived by applying a nonlinear shift according to equations (74)–(77). The nonlinear shift is seen to correspond to stretching the depth axis of the squeezed profiles. The effect of stretching is to locate interfaces that are mislocated in $\hat{\alpha}_P, \hat{c}_P, \hat{c}_S$ and $\hat{\rho}$ towards their correct location. Thus, in the absence of the actual P-wave velocity function, the nonlinear AVA analysis and depth imaging (stretch) algorithm extract the necessary information from the angle-dependent Born depth profile $\alpha_B(z)$.

Table 1. Fifteen-layer model, with reference velocities $c_{P0} = 1500$ m s^{-1} and $c_{S0} = 0$ m s^{-1} and density $\rho_0 = 1000$ kg m^{-3}. Here, z_n is the actual layer depth, $z_{nB}(0)$ is the layer depth from zero-angle Born constant-velocity imaging, $\hat{z}_n$ is the estimated actual layer depth, c_{Pn} is the actual layer P-wave velocity, $\hat{c}_{Pn}$ is the estimated layer P-wave velocity, $\varepsilon_{c_{Pn}}$ is relative error of the layer P-velocity estimate, c_{Sn} is the actual layer S-wave velocity, $\hat{c}_{Sn}$ is the estimated layer S-wave velocity, $\varepsilon_{c_{Sn}}$ is relative error of the layer S-velocity estimate, ρ_n is the actual layer density, $\hat{\rho}_n$ is the estimated layer density and ε_{ρ_n} is relative error of the layer density estimate.

n	z_n [m]	$z_{n\mathrm{B}}(0)$ [m]	$\hat{z}_n$ [m]	c_{Pn} [m s^{-1}]	$\hat{c}_{Pn}$ [m s^{-1}]	$\varepsilon_{c_{Pn}}$ [%]	c_{Sn} [m s^{-1}]	$\hat{c}_{Sn}$ [m s^{-1}]	$\varepsilon_{c_{Sn}}$ [%]	ρ_n [kg m^{-3}]	$\hat{\rho}_n$ [kg m^{-3}]	ε_{ρ_n} [%]
0	0	–	–	1500	–	–	0	–	–	1000	–	
1	300	300.0	300	1525	1525	0.0	50	49	−1.6	1025	1025	0.0
2	310	309.8	310	1550	1550	0.0	75	74	−0.8	1050	1050	0.0
3	320	319.5	320	1600	1600	0.0	100	99	−0.6	1100	1100	0.0
4	330	328.9	330	1675	1663	−0.7	300	276	−8.0	1150	1158	0.7
5	350	346.8	350	1775	1747	−1.6	500	462	−7.5	1225	1243	1.5
6	375	367.9	375	1900	1858	−2.2	700	653	−6.8	1300	1326	2.0
7	400	387.7	399	2000	1948	−2.6	900	861	−4.4	1600	1632	2.0
8	500	462.7	497	2000	1949	−2.5	1100	1059	−3.7	1900	1926	1.4
9	600	537.7	594	2200	2163	−1.7	1200	1172	−2.3	2000	1999	0.0
10	700	605.8	692	2600	2558	−1.6	1250	1254	0.3	2400	2355	−1.9
11	800	663.5	791	2300	2312	0.5	1300	1310	0.7	2400	2325	−3.1
12	1000	794.0	991	2200	2209	0.4	1250	1253	0.2	2300	2245	−2.4
13	1100	862.2	1093	2400	2341	−2.4	1200	1181	−1.6	2200	2203	0.1
14	1200	924.7	1190	2500	2444	−2.2	1250	1238	−0.9	2300	2284	−0.7

5. Model calculations

As an example of nonlinear direct AVA analysis and data-driven depth imaging with objective to estimate the depth-dependent velocities and density, from the single-scattering data, we consider the high-velocity/high-density contrast piecewise-constant 15-layer elastic medium displayed in figure 1 and listed in table 1. The reference velocities and density (in layer zero) are $c_{P0} = 1500$ m s^{-1}, $c_{S0} = 0$ m s^{-1} and $\rho_0 = 1000$ kg m^{-3}, respectively. The model has some properties that should be noted. The P-wave velocity is the same in layers eight and nine, whereas the density is the same in layers 11 and 12. In addition, there is a P-wave velocity increase but density decrease between layers 13 and 14.

In the example, perfect data are modelled directly in the time intercept-slowness domain with the algorithm described in appendix A. Observe that when the method be applied to real data recorded in the physical time-space domain, the data must go through three basic preprocessing steps. First, the data must be transformed from time-space to time intercept-slowness domain. This step can be performed by using the discrete fast Radon transform described in Ikelle and Amundsen (2005, appendix D). Second, multiples (multiple scattered waves) must be eliminated and third, the radiation pattern of the source described in equation (53) must be removed.

The primary reflection data from the model are plotted in figure 2 as traces as function of angle, ranging from 0° to 30°, for infinite bandwidth. The related angle-dependent Born potential is obtained by constant-velocity migration of each of the angle-traces. Figure 3 shows a selection of Born potential depth profiles for angles of 0°, 10°, 20° and 30°. Observe that the first interface is correctly positioned in depth (at $z_1 = 300$ m) in all the angle-profiles since the primary from the first interface always propagates with the reference velocity. The other

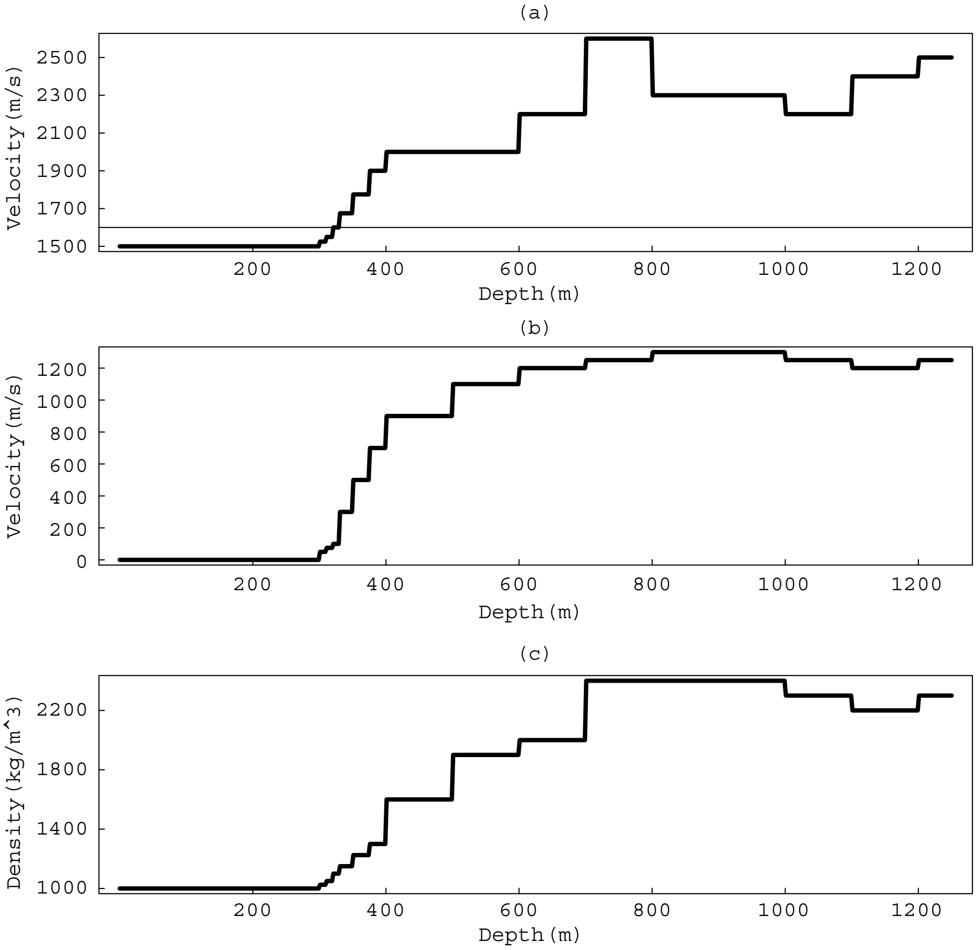

Figure 1. Actual model: (a) P-wave velocity, $c_P(z)$, (b) S-wave velocity, $c_S(z)$ and (c) density, $\rho(z)$. The model is listed in table 1.

interfaces are generally severely mislocated in depth. In addition, the image depth of these interfaces varies with angle, in the predictable way that the depth decreases with increasing angle. This behaviour we call interface residual moveout. Before any AVA analysis the interface residual moveout should be corrected so that all Born depth profiles have interface depths matching the interface depths of the zero-angle Born depth profile. Since the number of interfaces is the same in every Born depth profile, the residual moveout correction to apply can easily be found, for instance, by applying edge-detection techniques to each individual profile. Figure 4 shows the residual moveout-corrected angle gather of Born potential depth profiles corresponding to the gather in figure 3. In figure 4 gather, the interfaces are positioned at the same depth, but still the amplitudes of the residual moveout-corrected Born profiles differ as function of angle. The amplitude variation versus angle is the basis for estimating the squeezed depth-dependent velocity and density profiles. In the present study, we use only the moveout corrected angle-Born profiles at 0°, 10° and 20° to estimate the squeezed profiles. Figure 5 displays the squeezed velocity and density profiles. For comparison, the

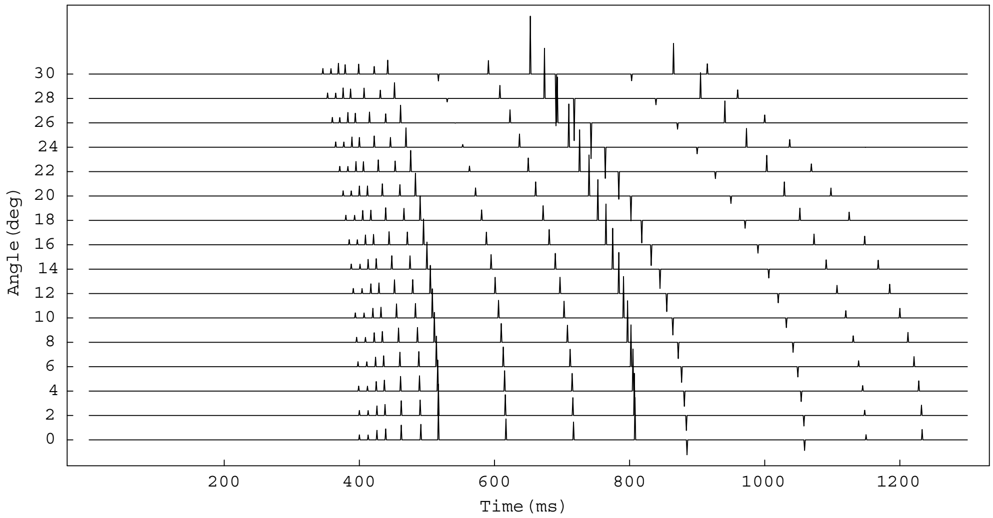

Figure 2. Angle gather of primary reflection events as function of time-intercept from the 15 layer model in figure 1.

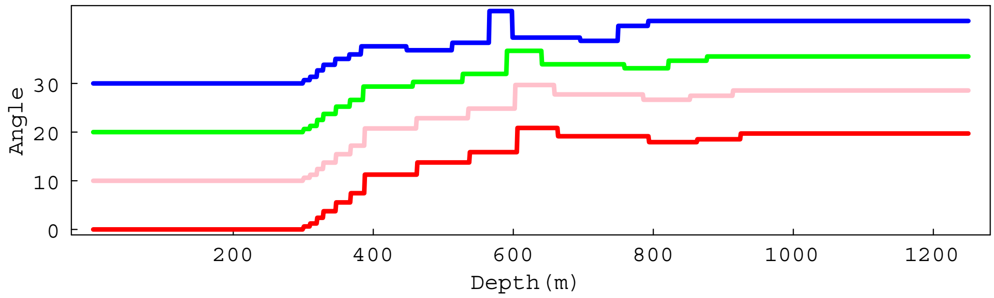

Figure 3. Angle gather of Born potential depth profiles. Red, pink, green and blue colours represent angles of incidence of 0°, 10°, 20° and 30°, respectively.

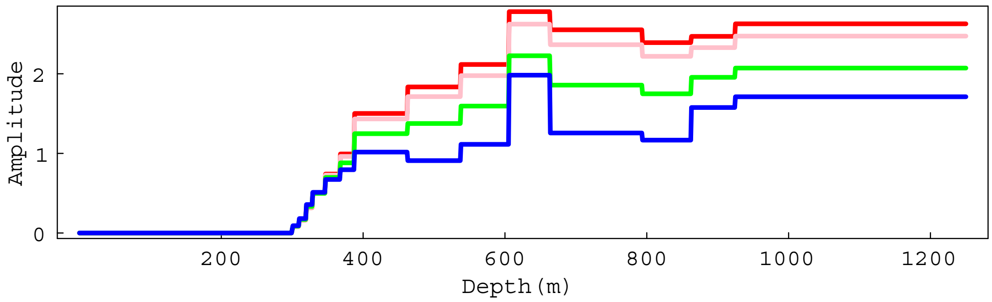

Figure 4. Moveout corrected angle gather of Born potential depth profiles corresponding to the gather in figure 3. Red, pink, green and blue colours represent angles of incidence of 0°, 10°, 20° and 30°, respectively.

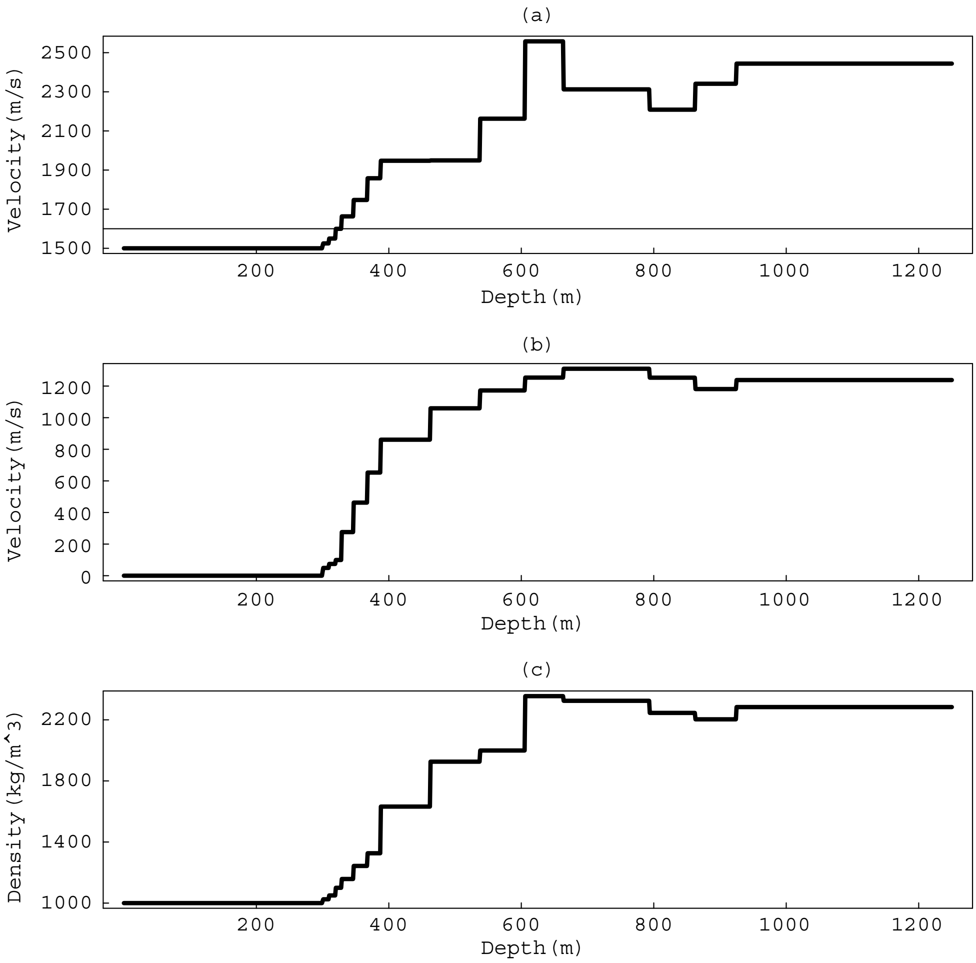

Figure 5. Nonlinear AVA inversion of the moveout-corrected angle-dependent Born potential (at 0°, 10° and 20°; see figure 4) gives squeezed (a) P-wave velocity, (b) S-wave velocity and (c) density.

zero-angle Born potential profile is shown in the same figure. Evidently, the depth of the interfaces of the squeezed profiles and the zero-angle Born profile matches. Observe that the estimated velocities and density, presented in table 1 together with the actual velocities and density c_{Pn}, c_{Sn} and ρ_n, respectively, display the same properties as the true parameters. The estimated layer velocities and density are at maximum approximately two-three per cent off.

From the squeezed P-wave potential, the actual velocities and density can be estimated in the WKBJ approximation by residual depth imaging, amounting to stretching the depth axis of the squeezed profiles using the amplitude of the squeezed P-wave velocity potential only. The results, both for velocities and density, are shown in figure 6. The estimated interface depth $\hat{z}_n$ is summarized in table 1.

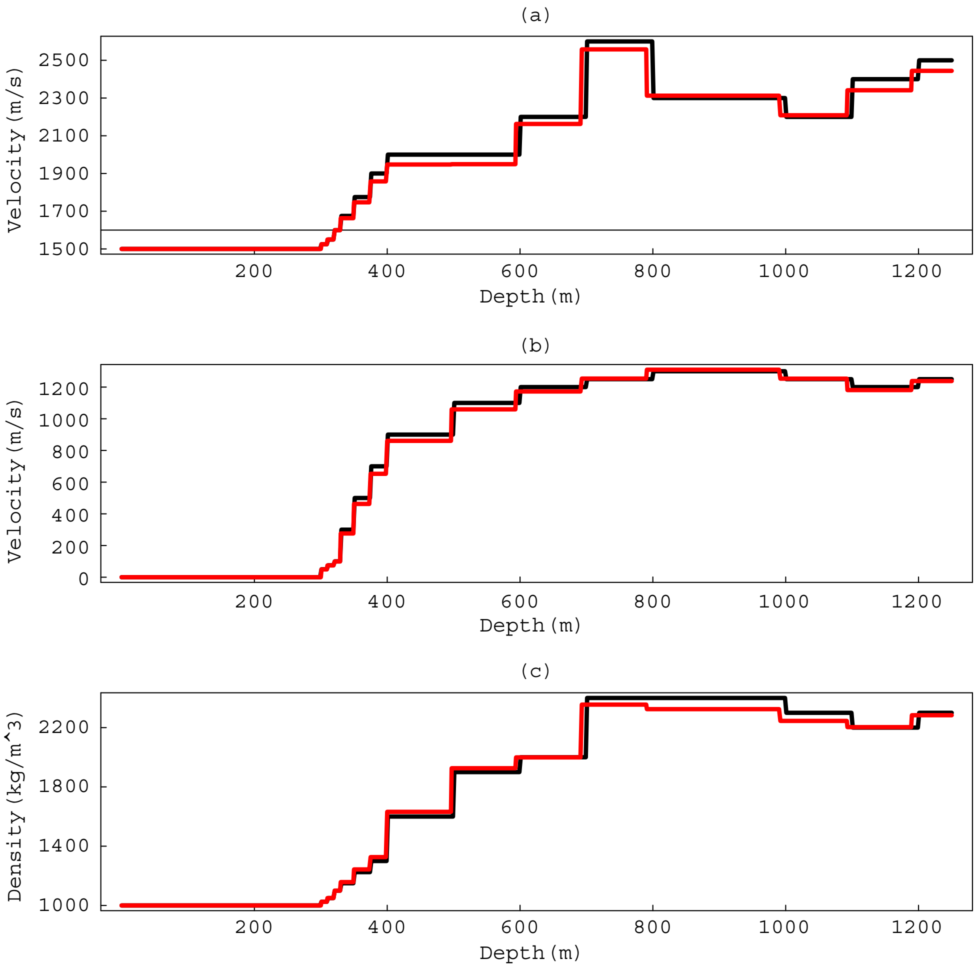

Figure 6. Residual depth imaging: stretching the squeezed profiles displayed in figure 5: (a) estimated P-wave velocity, (b) estimated S-wave velocity and (c) estimated density. The estimated curves are shown in red lines. For comparison, the actual models are displayed in black lines.

6. Conclusions

We have derived the forward model for elastic single P–P scattering from a depth-variable elastic medium in the WKBJ approximation. We have shown that the elastic inverse scattering problem can be solved in three main steps. First, from the single-scattering data in the time intercept-slowness domain, an angle-dependent Born potential profile is computed by constant-velocity imaging. Second, from the angle-dependent residual moveout-corrected Born potential depth profiles nonlinear direct AVA analysis is used to estimate depth-dependent squeezed velocity and density profiles. A squeezed profile contains information of the amplitude of the corresponding actual profile, not within the actual profile layer interfaces, but within the layer interfaces of the zero-angle profile of the Born potential. Third, the mislocated reflectors in the squeezed profiles are moved with high precision towards their correct spatial location by applying a nonlinear stretch function. The nonlinear AVA analysis and data-driven depth imaging require no information of the medium other than the angle-dependent Born potential. In the nomenclature of seismic data processing the three steps can be described by the sequence constant-velocity (partial) migration–inversion–residual migration.

A simple model example showed how the velocities and densities could be estimated in the WKBJ approximation, from the angle-dependent Born potential. Even for high-velocity and high-density contrast media (strong potentials), the theory gives an inverse scattering procedure that reconstructs the medium and its properties to a good approximation.

Acknowledgments

We thank StatoilHydro for allowing us to publish this work. The first author (LA) would like to thank Professor Arthur B Weglein for providing keen insight on his work on the inverse scattering series. We acknowledge constructive comments and suggestios from the reviewers.

Appendix A. Modelling of the PP-wave reflection response

We consider plane P-wave propagation with slowness (ray parameter) $p = \sin\theta_P/c_{P0}$ through a medium with $N + 1$ homogeneous layers with constant layer velocities c_{Pn} and c_{Sn}, and density ρ_n and thicknesses h_n. The source and receivers are both located at depth $z = 0$ in the zeroth layer which is the reference medium with velocities c_{P0} and c_{S0} and density ρ_0.

Together with proper boundary conditions, the differential equations (43) and (44) show that the wave field is made up of an infinite sum of reflections and refractions inside the medium (cf Bremmer (1951) and Santos *et al* (1996)). In what follows we show how to model the primary PP-wave reflection response, that is, the P-waves that are split off by reflection from the downgoing source P-wavefield when it is transmitted into the medium. To this end, it is necessary to define the P-wave reflection and transmission coefficients in the stack of layers (see appendix B). For a plane P-wave incident in layer $n - 1$, the reflection and transmission coefficients are denoted by $R_n(p)$ and $T_n^{(D)}(p)$. We will also need that a wave transmitted in the opposite direction, upwards from layer n into layer $n - 1$, has transmission coefficient $T_n^{(U)}(p)$. Then, the two-way transmission loss for a plane wave passing down and up through the interface at depth z_n is $T_n^{(D)}(p)T_n^{(U)}(p)$. The apparent velocity in layer n along the depth axis is

$$v_{Pn}(p) = \frac{c_{Pn}}{\sqrt{1 - (c_{Pn}p)^2}}.$$

When the source is initiated with unit strength a plane P-wave propagates downwards with velocity c_{P0} into the discontinuous, layered medium. At the boundary of the first layer, at depth $z_1 = h_0$, the incident wave which is represented by

$$D_0(\omega, p) = \exp[\mathrm{i}\omega h_0/v_{P0}(p)],$$

is split into [I] a refracted wave penetrating into this layer with amplitude $T_1^{(D)}(p)$ and represented by

$$D_1(\omega, p) = D_0(\omega, p)T_1^{(D)}(p)\exp[\mathrm{i}\omega(z - z_1)/v_{P1}(p)], \qquad z_1 < z < z_2,$$

and [II] a reflected wave with amplitude $R_1(p)$ returning to the receiver level where it is represented by

$$\Phi_1(\omega, p) = R_1(p)\exp[2\mathrm{i}\omega h_0/v_{P0}(p)].$$

The downgoing wave $D_1(\omega, p)$ will be split at the next interface at depth z_2 into a refracted wave

$$D_2(\omega, p) = D_1(\omega, p)T_2^{(D)}(p)\exp[\mathrm{i}\omega(z - z_2)/v_{P2}(p)], \qquad z_2 < z < z_3,$$

penetrating into layer 2, and a reflected wave which, after being refracted through the interface at depth z_1 returns to the receiver level with representation

$$\Phi_2(\omega, p) = R_2(p)T_1^{(D)}(p)T_1^{(U)}(p)\exp[2\mathrm{i}\omega h_1/v_{P1}(p)]\exp[2\mathrm{i}\omega h_0/v_{P0}(p)].$$

This procedure of splitting is repeated at each next interface. The chain of wave consisting of the sequence $\Phi_1, \Phi_2, \ldots, \Phi_N$ is the primary PP reflection response. One reflection response is obtained for each slowness.

In the frequency-slowness domain the N events of the dimensionless scattering amplitude can be is modelled as

$$\Phi_{PP}(\omega, p) = \sum_{n=1}^{N}\Phi_n(\omega, p) = \sum_{n=1}^{N}\hat{R}_n(p)\exp\left(2\mathrm{i}\omega\sum_{m=0}^{n-1}\frac{h_m}{v_{Pm}(p)}\right), \tag{A.1}$$

where each wave has the form of the product of an amplitude function and a delay function, both depending only on slowness. The frequency dependency comes only as a complex exponential due to the delay. The amplitude of the wave from the interface at depth z_n is the product of the plane-wave reflection coefficient at z_n and the transmission coefficients encountered by the wave, namely

$$\hat{R}_1(p) = R_1(p), \qquad \hat{R}_n(p) = R_n(p)\prod_{j=1}^{n-1}T_j^{(D)}(p)T_j^{(U)}(p), \qquad n = 2, 3, \ldots, N. \tag{A.2}$$

Performing an inverse Fourier transform over frequency, the dimensionless scattering amplitude in the time intercept-slowness domain becomes

$$\Phi_{PP}(t, p) = \sum_{n=1}^{N}\hat{R}_n(p)\delta(t - \tau_n(p)), \tag{A.3}$$

where $\delta(t)$ is the Dirac delta-function. The arrival time (called time-intercept) of the primary P-wave reflection from depth z_n is

$$\tau_n(p) = 2\sum_{m=0}^{n-1}\frac{h_m}{v_{Pm}(p)}.$$

(In time-space domain, τ is the time-intercept of the tangent line with slope p with the time axis.)

Appendix B. PP plane-wave reflection and transmission coefficients

This appendix gives the PP-wave reflection and transmission coefficients at a solid–solid and fluid–solid interface between layers 1 and 2 in terms of radial slowness p. The reader is referred to Ikelle and Amundsen (2005) for a derivation of the coefficients.

B.1. Solid–solid interface

Introduce the vertical slownesses

$$Q_{P1} = \sqrt{c_{P1}^{-2} - p^2} : \text{P-wave, layer 1}$$
$$Q_{S1} = \sqrt{c_{S1}{}^{-2} - p^2} : \text{S-wave, layer 1}$$
$$Q_{P2} = \sqrt{c_{P2}{}^{-2} - p^2} : \text{P-wave, layer 2}$$
$$Q_{S2} = \sqrt{c_{S2}{}^{-2} - p^2} : \text{S-wave, layer 2}$$

and the functions

$$
\begin{aligned}
d_1 &= 2p^2\Delta\mu(Q_{P1} - Q_{P2}) + (\rho_1 Q_{P2} + \rho_2 Q_{P1}) \\
d_2 &= 2p^2\Delta\mu(Q_{S1} - Q_{S2}) + (\rho_1 Q_{S2} + \rho_2 Q_{S1}) \\
d_3 &= p[2\Delta\mu(Q_{P1}Q_{S2} + p^2) - \Delta\rho] \\
d_4 &= p[2\Delta\mu(Q_{P2}Q_{S1} + p^2) - \Delta\rho] \\
c_1 &= 2p^2\Delta\mu(Q_{P1} + Q_{P2}) - (\rho_1 Q_{P2} - \rho_2 Q_{P1}) \\
c_3 &= -p[2\Delta\mu(Q_{P1}Q_{S2} - p^2) + \Delta\rho]
\end{aligned}
$$

with contrast parameters $\Delta\mu = \mu_1 - \mu_2$ and $\Delta\rho = \rho_1 - \rho_2$. The P-wave reflection and transmission coefficients for a downward-travelling incident plane wave in layer are

$$R = \frac{c_1 d_2 - c_3 d_4}{d_1 d_2 + d_4 d_3},$$

and

$$T^{(D)} = \frac{2\rho_1 Q_{P1} d_2}{d_1 d_2 + d_4 d_3}.$$

The transmission coefficient for an upward travelling incident plane wave in layer 2 is

$$T^{(U)} = \frac{2\rho_2 Q_{P2} d_2}{d_1 d_2 + d_4 d_3}.$$

B.2. Fluid–solid interface

The coefficients at a fluid–solid interface are found from those at the solid–solid interface in the limit $V_{S1} = 0$. Introducing

$$A_1 = (1 - 2p^2 c_{S2}{}^2)^2 = B^2, \qquad A_2 = 4p^2\rho_2 c_{S2}{}^4 Q_{S2}, \qquad B = 1 - 2p^2 c_{S2}{}^2,$$

we find

$$R = \frac{A_1\rho_2 Q_{P1} + A_2 Q_{P1} Q_{P2} - \rho_1 Q_{P2}}{A_1\rho_2 Q_{P1} + A_2 Q_{P1} Q_{P2} + \rho_1 Q_{P2}},$$

$$T^{(D)} = \frac{2B\rho_1 Q_{P1}}{A_1\rho_2 Q_{P1} + A_2 Q_{P1} Q_{P2} + \rho_1 Q_{P2}}$$

and

$$T^{(U)} = \frac{2B\rho_2 Q_{P2}}{A_1\rho_2 Q_{P1} + A_2 Q_{P1} Q_{P2} + \rho_1 Q_{P2}}.$$

Appendix C. The Born potential

By setting

$$\xi_P(z) \equiv 0 \tag{C.1}$$

in the forward model (55) the Born approximation model is obtained,

$$\Phi_{PP}(\omega, p) = \int_0^\infty \mathrm{d}z\, s_{PP}(p, z) \exp(2\mathrm{i}\omega q_P z), \tag{C.2}$$

where s_{PP} is given in equation (39). Performing a partial integration over the first term of Φ_{PP}, one obtains

$$\Phi_{PP}(\omega, p) = -\frac{\mathrm{i}\omega q_P}{2}\int_0^\infty \mathrm{d}z\, \alpha_{\mathrm{BPP}}(p, z)\exp(2\mathrm{i}\omega q_P z), \tag{C.3}$$

where the single-scattering Born potential

$$\alpha_{\mathrm{BPP}}(p, z) = \alpha_{\mathrm{BPPA}}(p, z) + \frac{1}{2\mathrm{i}\omega q_P}\alpha_{\mathrm{BPPE}}(p, z) \tag{C.4}$$

consists of acoustic and elastic-related parts, respectively,

$$\alpha_{\mathrm{BPPA}}(p, z) = -2\ln[r_\rho(z)\Gamma_P(p, z)] \tag{C.5}$$

and

$$\alpha_{\mathrm{BPPE}}(p, z) = 8p^2\rho^{-1}(z)\frac{\mathrm{d}}{\mathrm{d}z}\mu(z). \tag{C.6}$$

Our objective is now to invert equation (C.3) for the Born potential.

Consider the inverse Fourier transform over frequency of equation (C.3), that is,

$$\frac{2}{\pi}\int_{-\infty}^\infty \mathrm{d}\omega\exp(-\mathrm{i}\omega t)\frac{\Phi_{PP}(\omega, p)}{-\mathrm{i}\omega} = \int_0^\infty \mathrm{d}z'\frac{1}{2\pi}\int_{-\infty}^\infty \mathrm{d}\omega' \times\left[\alpha_{\mathrm{BPPA}}(p, z') + \frac{1}{\mathrm{i}\omega'}\alpha_{\mathrm{BPPE}}(p, z')\right]\exp\left[-\mathrm{i}\omega'\left(\frac{t}{2q_P} - z'\right)\right], \tag{C.7}$$

where $\omega' = 2\omega q_P$. By evaluating the integrals over frequency we obtain

$$4\int_{-\infty}^{2z/v_{P0}(p)} \mathrm{d}t\,\Phi_{PP}(t, p) = \int_0^\infty \mathrm{d}z'[\alpha_{\mathrm{BPPA}}(p, z')\delta(z - z') - \alpha_{\mathrm{BPPE}}(p, z')H(z - z')], \tag{C.8}$$

where $H(z)$ is the Heaviside function. We have introduced $z = t/(2q_P) = v_{P0}t/2$ and $v_{P0} = c_{P0}/\sqrt{1 - (c_{P0}p)^2} = c_{P0}/\cos\theta_P$ is the apparent velocity of the plane wave along the depth axis.

We now assume a discretized shear modulus model, with $z_i = \mathrm{i}\Delta z$, which is represented by

$$\mu(z) = \sum_{i=0}^\infty \Delta\mu(z_i)H(z - z_i), \tag{C.9}$$

where

$$\Delta\mu(z_i) = \mu(z_i) - \mu(z_{i-1}), \tag{C.10}$$

with derivative

$$\frac{\mathrm{d}}{\mathrm{d}z}\mu(z) = \sum_{i=0}^\infty \Delta\mu(z_i)\delta(z - z_i), \tag{C.11}$$

so that

$$\alpha_{\mathrm{BPPE}}(p, z) = 8p^2\sum_{i=0}^\infty \frac{\Delta\mu(z_i)}{\rho^{-1}(z_i)}\delta(z - z_i). \tag{C.12}$$

Equation (C.8) then becomes

$$4\int_{-\infty}^{2z/v_{P0}(p)} \mathrm{d}t\,\Phi_{PP}(t, p) = \alpha_{\mathrm{BPPA}}(p, z) - 8p^2\sum_{i=0}^\infty \frac{\Delta\mu(z_i)}{\rho(z_i)}\int_0^\infty \mathrm{d}z'H(z - z')\delta(z' - z_i). \tag{C.13}$$

Inserting equation (C.5) and evaluating the integral on the right-hand side of equation (C.13) yield

$$4\int_{-\infty}^{2z/v_{P0}(p)} \mathrm{d}t\,\Phi_{PP}(t,p) = -2\ln[r_\rho(z)\Gamma_P(p,z)] - 8p^2\sum_{i=0}^{\infty}\frac{\Delta\mu(z_i)}{\rho(z_i)}H(z-z_i), \tag{C.14}$$

The Born potential, per definition, is Amundsen *et al* (2006)

$$\alpha_{\mathrm{BPP}}(p,z) = 4\int_{-\infty}^{2z/v_{P0}(p)} \mathrm{d}t\,\Phi_{PP}(t,p). \tag{C.15}$$

Equation (C.15) which is a key equation in the inversion procedure is known as constant-velocity migration or linear migration–inversion.

Finally, by introducing

$$f_{\mu,\rho}(z) = \exp\left[4p^2\sum_{i=0}^{\infty}\frac{\Delta\mu(z_i)}{\rho(z_i)}H(z-z_i)\right], \tag{C.16}$$

the Born potential can be written compactly as

$$\alpha_{\mathrm{BPP}}(z) = -2\ln[r_\rho(z)\Gamma_P(z)f_{\mu,\rho}(z)]. \tag{C.17}$$

In section 4.2, we shall see that the Born potential is the ticket for determining the elastic parameters.

C.1. Depth of interfaces after constant-velocity migration

After constant-velocity migration primary reflection events are placed at depths computed linearly using their traveltimes together with the constant reference velocity. This is readily verified by substituting the primary reflection response (A.3) into equation (C.15). One obtains

$$\alpha_{\mathrm{BPP}}(p,z) = 4\sum_{n=1}^{N}\hat{R}_n(p)H(z-z_{n\mathrm{BPP}}(p)), \tag{C.18}$$

where $z_{n\mathrm{BPP}}$ is the depth at which the reference velocity c_{P0} images the nth reflector,

$$z_{n\mathrm{BPP}}(p) = v_{P0}(p)\sum_{m=0}^{n-1}\frac{h_m}{v_{Pm}(p)}.$$

The Born-estimated thickness of layer m thus is

$$h_{mB}(p) = \frac{v_{P0}(p)}{v_{Pm}(p)}h_m.$$

Observe that the first reflector is imaged at its correct depth for all slowness (or angle) traces,

$$z_{1\mathrm{BPP}} = h_0 = z_1,$$

which is obvious since $\alpha_P(z) = 0$ for $z < z_1$.

References

Amundsen L, Reitan A, Arntsen B and Ursin B 2006 Acoustic nonlinear amplitude versus angle inversion and data-driven depth imaging in stratified media derived from inverse scattering approximations *Inverse Problems* **22** 1921–45

Amundsen L, Reitan A, Helgesen H K and Arntsen B 2005 Data-driven inversion/depth imaging derived from approximations to one-dimensional inverse acoustic scattering *Inverse Problems* **21** 1823–50

Bremmer H 1951 The W.K.B. approximation as a first term of a geometric-optical series *The Theory of Electromagnetic Waves, A Symposium* (New York: Interscience) pp 169–79

Cohen J and Bleistein N 1979 Velocity inversion procedure for acoustic waves *Geophysics* **44** 1077–87

dos Santos L T, Ursin B and Tygel M 1996 Wave series expansion for a stratified fluid *Russ. Geol. Geophys.* **37** 23–45

Ikelle L T and Amundsen L 2005 *Introduction to Petroleum Seismology* (Tulsa, OK: Society of Exploration Geophysics)

Innanen K A 2003 Methods for the treatment of acoustic and absorptive/dispersive wave field measurements *PhD Thesis* University of British Columbia

Rayleigh L 1950 *The Theory of Sound* (New York: Dover)

Razavy M 1975 Determination of the wave velocity in an inhomogeneous medium from the reflection coefficient *J. Acoust. Soc. Am.* **58** 956–63

Shaw S A 2005 An inverse scattering series algorithm for depth imaging of reflection data from a layered acoustic medium with an unknown velocity model *PhD Thesis* University of Houston

Symes W W 1981 The inverse reflection problem for a smoothly stratified elastic medium *SIAM J. Math. Anal.* **12** 421–53

Ursin B 1983 Review of elastic and electromagnetic wave propagation in layered media *Geophysics* **48** 1063–81

Ursin B 1984 Seismic migration using the WKB approximation *Geophys. J. R. Astron. Soc.* **79** 339–52

Weglein A B, Amundsen L, Liu F, Innanen K, Nita B, Zhang J, Ramirez A and Otnes E 2007 Inverse scattering subseries direct removal of multiples and depth imaging and inversion of primaries without subsurface information: strategy and recent advances *Expanded Abstracts, 77th Ann. Internat. Mtg., Soc. Expl. Geophys.*

Weglein A B, Araújo R V, Carvalho P M, Stolt R H, Matson K H, Coates R T, Corrigan D, Foster D J, Shaw S A and Zhang H 2003 Inverse scattering series and seismic exploration *Inverse Problems* **19** R27–83

Weglein A B, Boyse W E and Anderson J E 1981 Obtaining three-dimensional velocity information directly from reflection seismic data: an inverse scattering formalism *Geophysics* **46** 1116–20